Numerical Investigation on Effects of Solid Grain Concentrations on Cavitation Evolution Around NACA0015 Hydrofoil

Xiangdong Han[1], Chao Wang[2], Youchao Yang[2], Weiguo Zhao[3], and Pengjun Fan[4(✉)]

[1] School of Civil Engineering, Nanchang Institute of Technology, Nanchang 330044, China
[2] Chongqing Pump Industry Co., Ltd., Chongqing 400033, China
[3] College of Energy and Power Engineering, Lanzhou University of Technology, Lanzhou 730050, China
[4] Machine Industry Lanzhou Petrochemical Equipment Inspection Institute Co., LTD, Lanzhou 730070, China
fanpengjun@lanpec.com

Abstract. Effects of solid grains with different concentrations on cavitation evolution around NACA0015 hydrofoil were investigated. The concentrations were 5%, 10%, and 20%. Variations of averaged lift and drag coefficients and lift-drag ratio under all concentration conditions were analyzed; corresponding evolution processes of cavitation bubbles were discussed. Results indicated that with the growing of the concentration, averaged lift coefficient decreased, averaged drag coefficient increased, and lift-drag ratio reduced. They were less than their counterparts in pure water cavitation flow. Cavitation bubble evolution process and distribution of streamlines were various under the effects of the concentration. With the growing of the concentration, shedding dominant frequency and Strouhal number decreased.

Keywords: Solid grain-pure water-cavitation flow · Solid grain concentration · NACA0015 hydrofoil · Numerical simulation

1 Introduction

Cavitation, one kind of particularly complex multiphase flow [1], occurs in various fluid-handling devices, such as pump [2], valve [3], and nozzle [4]. The evolution process and related influence factors have been deeply investigated [5]. Detrimental effects caused by cavitation are well-known in engineering fields [6].

However, cavitation also has their significant merits; for example, cavitating water jet could be employed to perform rock mining [7]. Under some special conditions that environmental temperature is particularly low, cavitating water jet intensity is not strong enough to achieve it. Some investigators added solid grains to cavitating water jet to enhance the intensity; it is the solid grain-pure water-cavitation flow (SG-PW-CF), one solid-liquid-vapor with mass transfer three-phase flow [8], different from pure water cavitation flow (PW-CF).

L. Yan and J. Na (Eds.): ICFPMCE 2022, AHE 10, pp. 273–281, 2023.
https://doi.org/10.2991/978-94-6463-022-0_24

Some scholars have investigated interactions between solid grains with cavitation bubbles. Xu et al. [9] discussed cavitation bubble collapse characteristics under the interaction between solid grains with cavitation bubbles; their dimensionless distance and size ratio had remarkable effects on the collapse. Teran et al. [10] performed experimental and numerical studies on the interactions between hard solid grains with different sizes and materials with cavitation bubbles near solid wall; they got that when solid grains were above cavitation bubbles, sizes and densities of grains performed significant effects on the motion. Dunstan and Li [11] numerically investigated the interactions of one single cavitation bubble with many solid grains and one grain with many bubbles; micro jet caused by cavitation bubble collapse made the grains accelerated.

Inspired by above mentioned investigations, numerical simulation of SG-PW-CF around NACA0015 hydrofoil was achieved. The mean diameter was 0.05 mm and the concentrations were 5%, 10%, and 20%, respectively.

2 Mathematical Model

2.1 Fundamental Equations

In the numerical simulation process of SG-PW-CF around NACA0015 hydrofoil, water was the primary phase. Vapor and solid grains were secondary phase. Phase change occurred between water with vapor; for solid grains, this process was ignored. Continuity equation, momentum equation, transportation equations for vapor and solid grains, and relative velocity equation [12] are shown as follows.

$$\frac{\partial \rho_{\mathrm{m}}}{\partial t} + \frac{\partial \left(\rho_{\mathrm{m}} u_j\right)}{\partial x_j} = 0 \tag{1}$$

$$\frac{\partial (\rho_{\mathrm{m}} u_i)}{\partial t} + \frac{\partial \left(\rho_{\mathrm{m}} u_i u_j\right)}{\partial x_j} = -\frac{\partial p}{\partial x_i} + \frac{\partial}{\partial x_j}\left(\mu_{\mathrm{m}} \frac{\partial u_i}{\partial x_j}\right) \tag{2}$$

$$\frac{\partial \rho_{\mathrm{v}} \alpha_{\mathrm{v}}}{\partial t} + \frac{\partial \left(\rho_{\mathrm{v}} \alpha_{\mathrm{v}} u_j\right)}{\partial x_j} = m_{\mathrm{c}} - m_{\mathrm{e}} \tag{3}$$

$$\frac{\partial \rho_{\mathrm{s}} \alpha_{\mathrm{s}}}{\partial t} + \frac{\partial \left(\rho_{\mathrm{s}} \alpha_{\mathrm{s}} u_j\right)}{\partial x_j} = 0 \tag{4}$$

$$\mathbf{v}_{\mathrm{pq}} = \mathbf{v}_{\mathrm{p}} - \mathbf{v}_{\mathrm{q}} \tag{5}$$

where ρ_{m}, ρ_{v}, and ρ_{s} are the densities of mixture, vapor, and solid grains. α_{v} and α_{s} are the volume fractions of vapor and solid grains. u is the mixture velocity and x is the coordinate; i and j are subscripts. μ_{m} is the mixture viscosity. p is the pressure. m_{e} and m_{c} are source terms of evaporization and condensation. t is time. $\mathbf{V}_{\mathrm{pq}}$ is the relative velocity vector between primary phase with secondary phase; $\mathbf{V}_{\mathrm{p}}$ is the secondary phase velocity vector and $\mathbf{V}_{\mathrm{q}}$ is the corresponding one for primary phase.

2.2 Turbulence Model

SST k-ω turbulence model [13] was used to solve the turbulent flow in SG-PW-CF. It integrated the merits of k-ε model and standard k-ω model. This model was particularly robust. Transportation equations for turbulent kinetic energy and specific dissipation rate are given in the following equations.

$$\rho_{\mathrm{m}}\frac{\partial k}{\partial t}+\rho_{\mathrm{m}}\overline{u_j}\frac{\partial k}{\partial x_j}=P_k-\rho_{\mathrm{m}}\beta_*\omega k+\frac{\partial}{\partial x_j}\left[\left(\mu+\frac{\mu_{\mathrm{t}}}{\sigma_k}\right)\frac{\partial k}{\partial x_j}\right] \tag{6}$$

$$\begin{aligned}\rho_{\mathrm{m}}\frac{\partial \omega}{\partial t}+\rho_{\mathrm{m}}\overline{u_j}\frac{\partial \omega}{\partial x_j}=&\alpha P_\omega-\rho_{\mathrm{m}}\beta_*\omega^2+\frac{\partial}{\partial x_j}\left[\left(\mu+\frac{\mu_{\mathrm{t}}}{\sigma_\omega}\right)\frac{\partial \omega}{\partial x_j}\right]\\&+2\rho_{\mathrm{m}}(1-F_1)\frac{1}{\sigma_{\omega_{\mathrm{out}}}\omega}\frac{\partial k}{\partial x_j}\frac{\partial \omega}{\partial x_j}\end{aligned} \tag{7}$$

where k is turbulent kinetic energy and P_k is the corresponding production term. ω is the specific dissipation rate and P_ω is the corresponding production term. μ is dynamic viscosity; μ_{t} is turbulent viscosity. F_1 is the blending function. σ_k and σ_ω are empirical coefficients. β_* and $\sigma_{\omega\mathrm{out}}$ are 0.09 and 1.168.

Turbulent viscosity in SST k-ω turbulence model was modified according to the method employed in RNG k-ε turbulence model [14].

2.3 Cavitation Model

Cavitation model proposed by Schnerr and Sauer [15] was employed to perform the mass transfer between water with vapor in SG-PW-CF. The most remarkable merit was that empirical coefficients did not exist in this model. Therefore, the accuracy was relatively high. Evaporization and condensation source terms are shown as follows.

$$m_{\mathrm{e}}=\frac{\rho_{\mathrm{l}}\rho_{\mathrm{v}}}{\rho_{\mathrm{m\text{-}l\text{-}v}}}\alpha_{\mathrm{v}}(1-\alpha_{\mathrm{v}})\frac{3}{r_{\mathrm{b}}}\sqrt{\frac{2}{3}\frac{p_{\mathrm{v}}-p}{\rho_{\mathrm{l}}}} \tag{8}$$

$$m_{\mathrm{c}}=\frac{\rho_{\mathrm{l}}\rho_{\mathrm{v}}}{\rho_{\mathrm{m\text{-}l\text{-}v}}}\alpha_{\mathrm{v}}(1-\alpha_{\mathrm{v}})\frac{3}{r_{\mathrm{b}}}\sqrt{\frac{2}{3}\frac{p-p_{\mathrm{v}}}{\rho_{\mathrm{l}}}} \tag{9}$$

where ρ_{l} is the density of water; r_{b} is cavitation bubble radius. p_{v} is saturated vapor pressure. $\rho_{\mathrm{m\text{-}l\text{-}v}}$ is the mixture density of water and vapor, which is defined as follows:

$$\rho_{\mathrm{m\text{-}l\text{-}v}}=\rho_{\mathrm{l}}\alpha_{\mathrm{l}}+\rho_{\mathrm{v}}\alpha_{\mathrm{v}} \tag{10}$$

where α_{l} is the volume fraction of water.

3 Numerical Simulation Setup

3.1 Physical Model

NACA0015 hydrofoil was employed to perform the numerical simulation of SG-PW-CF. Angle of attack was $\alpha = 8°$ and chord length was $c = 0.1$ m. Corresponding computational domain is shown in Fig. 1. Length between leading ledge of the hydrofoil with circular-arc inlet was $5c$ and it was $10c$ for trailing ledge with outlet. Distance between the foil center with upper or lower boundaries was $6c$.

3.2 Mesh Generation

Structured C-type mesh was utilized to discretize the computational domain. Meshes around the hydrofoil surface and in the wake region were refined. The total number was 46820. It is shown in Fig. 2.

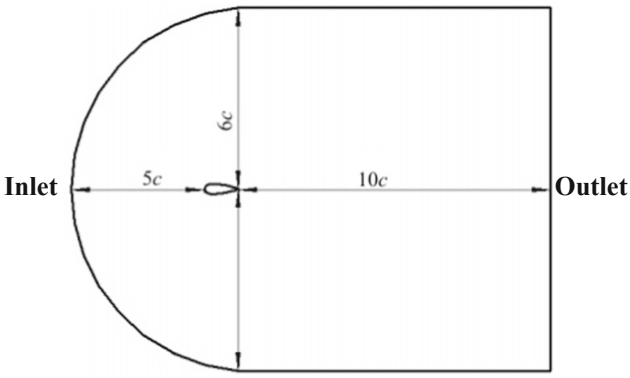

Fig. 1. The computational domain.

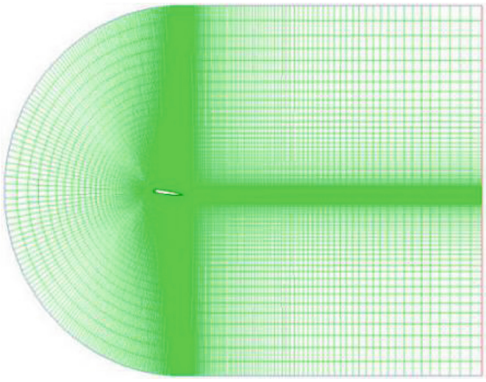

Fig. 2. Meshes of the computational domain.

3.3 Boundary Conditions

Velocity was set at the inlet, taken as 10 m/s. For the outlet, it was pressure-outlet condition; it could be calculated according to the cavitation number $\sigma = 0.5$. Upper and lower boundaries were non-slip conditions. Time step was $\Delta t = 1.0 \times 10^{-4}$ s. The total step was 5000.

4 Results and Discussion

4.1 Variations of Hydrodynamic Performances

Lift and drag coefficients and corresponding lift-drag ratio [16] reflect the hydrodynamic performances of the hydrofoil. They are calculated as follows:

$$C_L = \frac{L}{0.5\rho V_\infty^2 A} \tag{11}$$

$$C_D = \frac{D}{0.5\rho V_\infty^2 A} \tag{12}$$

$$K = \frac{C_L}{C_D} \tag{13}$$

where C_L is lift coefficient and C_D is drag coefficient. L is lift and D is drag. V_∞ is inflow velocity in far-away field. A is hydrofoil projected area. K is lift-drag ratio.

In PW-CF, the calculated averaged C_L was 0.295. For SG-PW-CF with $\alpha_\mathrm{s} = 5\%$, 10%, and 20%, they were 0.216, 0.195, and 0.167. They decreased with the increase of solid grain concentration.

For averaged C_D, it is 0.091 in PW-CF. They were 0.085, 0.086, and 0.087 in SG-PW-CF, respectively; variation trend was contrary to that of averaged C_L.

The calculated K for PW-CF was 3.241. In SG-PW-CF, they were 2.541, 2.267, and 1.920; they steadily decreased as the concentration grew (Fig. 3).

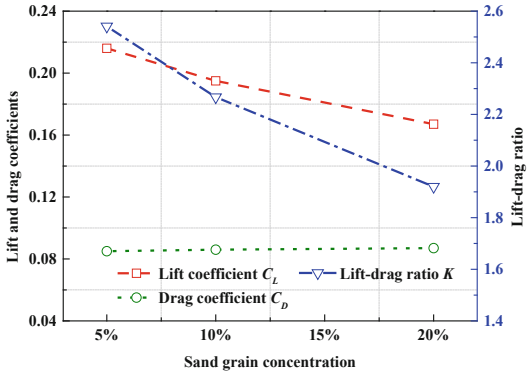

Fig. 3. Variations of averaged lift and drag coefficients and lift-drag ratio.

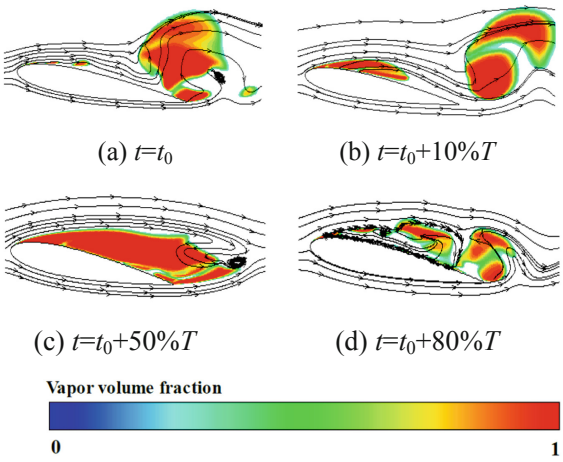

Fig. 4. Cavitation bubble evolution process in PW-CF.

4.2 Evolution of Cavitation Bubbles

Figure 4 is the cavitation bubble evolution process and the distribution of streamlines in PW-CF around NACA0015 hydrofoil from $t = t_0$ to $t = t_0 + 80\%T$. Figure 5 is the corresponding ones of SG-PW-CF under diverse concentration conditions. Both for PW-CF and SG-PW-CF, cavitation bubbles and streamlines had significant variations with time. From $t = t_0$ to $t = t_0 + 10\%T$, cavitation bubbles developed gradually. In PW-CF, streamlines were smooth and vortices were barely existed. Under $\alpha_s = 5\%$, streamlines were relatively smooth. For $\alpha_s = 10\%$ and 20%, streamlines became disorder and vortices appeared near the trailing ledge. From $t = t_0 + 10\%T$ to $t = t_0 + 80\%T$, cavitation bubbles evaluated constantly. At $t = t_0 + 50\%T$, cavitation bubbles became large, especially for $\alpha_s = 5\%$. Compared with other conditions, length and thickness under $\alpha_s = 10\%$ were the smallest. For $t = t_0 + 80\%T$, strengths of the vortices at $\alpha_s = 10\%$ and 20% were particularly intense. In PW-CF, the strength was relatively weak. On the other hand, the shedding dominant frequency and Strouhal number were calculated. For PW-CF, they were 20 Hz and 0.256. Under SG-PW-CF with $\alpha_s = 5\%$, 10%, and 20%, the frequencies were 20 Hz, 16.7 Hz, and 6.7 Hz. The Strouhal numbers were 0.227, 0.195, and 0.0804. They reduced with the increase of the concentration.

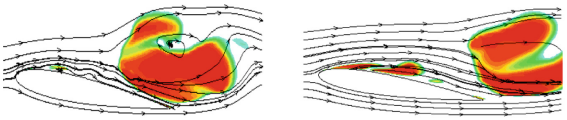

(a) $t=t_0$ (b) $t=t_0+10\%T$

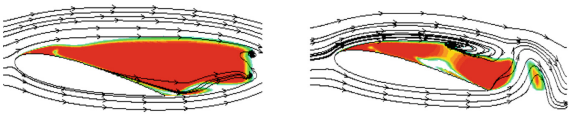

(c) $t=t_0+50\%T$ (d) $t=t_0+80\%T$

(1) SG-PW-CF with α_s=5%

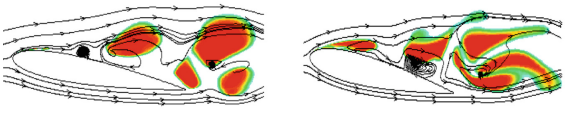

(a) $t=t_0$ (b) $t=t_0+10\%T$

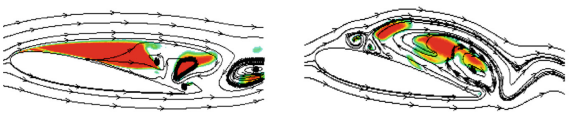

(c) $t=t_0+50\%T$ (d) $t=t_0+80\%T$

(2) SG-PW-CF with α_s=10%

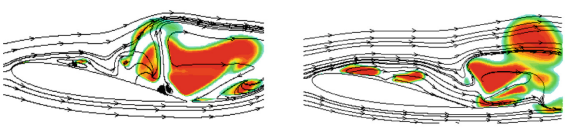

(a) $t=t_0$ (b) $t=t_0+10\%T$

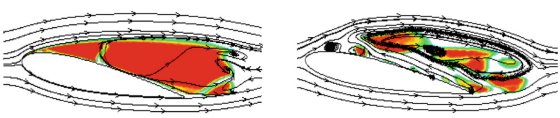

(c) $t=t_0+50\%T$ (d) $t=t_0+80\%T$

(3) SG-PW-CF with α_s=20%

Fig. 5. Cavitation bubble evolution process in SG-PW-CF.

5 Conclusions

SG-PW-CF with solid grain concentrations of 5%, 10%, and 20% around NACA0015 hydrofoil was numerically simulated to investigate the action modes of the concentrations. Variation laws of averaged lift and drag coefficients and lift-drag ratio were got. Variation characteristics of cavitation bubble evolution processes were determined. Main conclusions were as follows:

(1) In SG-PW-CF, averaged lift and drag coefficients and lift-drag ratio were less than those of PW-CF. Averaged lift coefficient reduced, averaged drag coefficient increased, and lift-drag ratio decreased with the growing of the concentration.
(2) Effects of different solid grain concentrations on cavitation bubble evolution and distribution of streamlines were different. The shedding dominant frequency and Strouhal number decreased with the growing of the concentration.

Acknowledgments. The investigation was financially supported by National Natural Science Foundation of China (Grant No. 52169018).

References

1. Ghadimi, A., Ghassemi, H.: Comparative assessment of hydrodynamic performance of two-dimensional Naca0012 and Naca6612 hydrofoils under different cavitation and non-cavitation conditions. Int. J. Hydromechatron. **3**(4), 349–367 (2020). https://doi.org/10.1504/IJHM.2020.112161
2. d'Agostino, L., Salvetti, M.V.: Fluid Dynamics of Cavitation and Cavitating Turbopumps, Springer, Wien (2010)
3. Scheidl, R., Scherrer, M., Zagar, P.: The buckling beam as actuator element for on-off hydraulic micro valves. Int. J. Hydromechatron. **4**(1), 55–68 (2021). https://doi.org/10.1504/IJHM.2021.114172
4. Dai, Y.X., Zhang, X.F., Zhang, G.Q., Cai, M.X., Zhou, C.H., Ni, Z.J.: Numerical analysis of influence of cavitation characteristics in nozzle holes of curved diesel engines. Flow Meas. Instrum. **85**, 102172 (2022). https://doi.org/10.1016/j.flowmeasinst.2022.102172
5. Koukouvinis, F., Gavaises, M.: Cavitation and Bubble Dynamics: Fundamentals and Applications. Academic Press (2021)
6. Kang, C., Liu, H.X., Song, L.B., Zhang, S.: Cavitation Erosion. Science Press (2020)
7. Washio, S.: Recent Developments in Cavitation Mechanisms. Woodhead Publishing (2018)
8. Zhao, W.G., Han, X.D., Li, R.N., Zheng, Y.J., Wang, Y.Y.: Effects of size and concentration of silt particles on flow and performance of a centrifugal pump under cavitating conditions. Mod. Phys. Lett. B **31**(34), 1750312 (2017). https://doi.org/10.1142/S0217984917503122
9. Xu, W.L., Zhang, Y.L., Luo, J., Zhang, R.A.Q., Zhai, Y.W.: The impact of particles on the collapse characteristics of cavitation bubbles. Ocean Eng. **131**, 15–24 (2017). https://doi.org/10.1016/j.oceaneng.2016.12.025
10. Teran, L.A., Rodríguez, S.A., Laín, S., Jung, S.: Interaction of particles with a cavitation bubble near a solid wall. Phys. Fluids **30**, 123304 (2018). https://doi.org/10.1063/1.5063472
11. Dunstan, P.J., Li, S.C.: Cavitation enhancement of silt erosion: numerical studies. Wear **268**(7–8), 946–954 (2010). https://doi.org/10.1016/j.wear.2009.12.036

12. Sharma, A.: Introduction to Computational Fluid Dynamics: Development, Application and Analysis. Springer (2021)
13. Wilcox, D.C.: Simulation of transition with a two-equation turbulence model. AIAA J. **32**(2), 247–255 (1994). https://doi.org/10.2514/3.59994
14. Coutier-Delgosha, O., Stutz, B., Vabre, A., Legoupil, S.: Analysis of cavitating flow structure by experimental and numerical investigations. J. Fluid Mech. **578**, 171–222 (2007). https://doi.org/10.1017/S0022112007004934
15. Schnerr, G.H., Sauer, J.: Physical and numerical modeling of unsteady cavitation dynamics. In: Proceedings of the 4th International Conference on Multiphase Flow, Louisiana, USA (2001)
16. Cengel, Y.A., Cimbala, J.M.: Fluid Mechanics: Fundamentals and Applications (Fourth Edition in SI Units), McGraw-Hill Education (2019)